American Mineralogist, Volume 73, pages 1074–1088, 1988

Laser Raman microprobe analysis of experimentally re-equilibrated fluid inclusions in olivine: Some implications for mantle fluids

JILL DILL PASTERIS

Department of Earth and Planetary Sciences and McDonnell Center for the Space Sciences, Washington University, Box 1169, St. Louis, Missouri 63130, U.S.A.

B. J. WANAMAKER*

Department of Geological and Geophysical Sciences, Princeton University, Princeton, New Jersey 08544, U.S.A.

ABSTRACT

Polished wafers of San Carlos olivine, containing fluid inclusions, were heat treated at temperatures up to 1400 °C at oxygen fugacities within the stability field of Fo_{90}, that is, approximately between the fayalite-magnetite-quartz and iron-wüstite buffers. The f_{O_2} was controlled by appropriate mixtures of H_2 and CO_2 or CO and CO_2. Analysis by microthermometry (MT) and laser Raman microprobe (LRM) showed all of the fluid inclusions to consist of pure CO_2 before the experiments were performed. However, when these same inclusions were checked by MT after 1 to 161 h of heat treatment, melting-point depressions (cf. −56.6 °C for pure CO_2) were observed. The lowest final melting temperatures, about −63.5 °C, were recorded for samples treated at the lowest f_{O_2} values. LRM analyses showed many of these re-equilibrated inclusions to consist of mixtures of CO and CO_2, ranging from trace CO to 44 ± 5 mol% CO. The inclusions treated at the lowest f_{O_2} values also contain moderately well crystallized graphite, as revealed by LRM analysis, but not detectable optically. Rapid reactions obviously have occurred among (1) the initially high-f_{O_2}, pure-CO_2 fluid inclusions, (2) the natural olivine with its inherent Fe^{2+}-Fe^{3+} ratio and defect abundance, and (3) the reducing H_2-CO_2 and CO-CO_2 mixtures in the furnace gas. Clearly, oxidation-reduction and diffusion are involved in the re-equilibration. The rapidity of the reactions seems to rule out ionic diffusion, including pipe diffusion along dislocations. The most likely mechanism of re-equilibration involves the diffusion of metal vacancies (point-defect diffusion) within the host olivine. Changes in defect concentrations in the solid, in response to the externally imposed f_{O_2}, resulted in the transfer of oxygen from the inclusion fluid to the surrounding solid. This transfer resulted in the production of CO: $2CO_2 = 2CO + O_2$. The precipitation of graphite in the lowest-f_{O_2} experiments is significant in that the combined reactions $CO_2 = C + O_2$ and $2\,CO = CO_2 + C$ prevented the inclusion fluid from exceeding about 42 mol% CO, even though the predicted compositions were up to 90 mol% CO (considering only the equilibrium $2CO_2 = 2CO + O_2$). In other words, the inclusions became internally buffered along the CCO buffer. The rapid re-equilibration of fluid inclusions (and their host minerals) suggests the unlikelihood of detecting trapped fluids whose compositions represent early magmatic processes deep in the upper mantle. It also suggests that some further cautions are required in the interpretation of "inherent" mineral characteristics such as defect concentrations and intrinsic oxygen fugacity.

INTRODUCTION

It has been recognized that volatile species of C-O-H-S composition must exist in the mantle in some physical state (free volatile phase, dissolved in melts, in interstitial solid solutions, incorporated as complex anions in minerals). Physical evidence of the *evolved* compositions of the mantle volatiles exists in fluid inclusions trapped in mantle xenoliths (Roedder, 1965; Murck et al., 1978; Bergman, 1981; Andersen et al., 1984) and in volatiles released from active volcanoes (e.g., Gerlach and Nordlie, 1975). Our increasing understanding of high-temperature and high-pressure phase equilibria has made clear the significance of these volatiles in the partial melting of mantle peridotite (e.g., Eggler, 1976; Wyllie, 1980; Taylor and Green, 1987; Green et al., 1987), in the transport of major and trace elements and the mechanism of metasomatism (Wendlandt and Harrison, 1979; Spera and Bergman, 1980; Ryabchikov et al., 1982; Mysen, 1983; Schneider and Eggler, 1986; Eggler, 1987), and in the transport of heat (Spera, 1981).

* Present address: Lawrence Livermore National Laboratory, L201, P.O. Box 808, Livermore, California 94550, U.S.A.

0003–004X/88/0910–1074$02.00

Combining the data from trapped fluids with the inferences from experimental and theoretical petrology has led to the consensus that the volatile component in the mantle most likely is a mixture predominantly of CO_2, H_2O, CH_4, and sulfur species. For the pressures and temperatures of the upper mantle, CO_2 and H_2O would be the dominant species at oxygen fugacities equal to or greater than the wüstite-magnetite buffer. At still lower f_{O_2} values, as reported in type I xenoliths investigated by Arculus et al. (1984), the speciation would be dominantly CH_4-H_2O (Eggler and Baker, 1982). Furthermore, at pressures greater than about 22 kbar, CO_2-H_2O volatiles would not exist as a free mobile phase, but rather would be stabilized in carbonated and hydrated minerals or dissolved in coexisting melt (Olafsson and Eggler, 1983). If *reduced* species such as CH_4 instead are stable (see Taylor and Green, 1987; Green et al., 1987), then the volatiles are free from the constraint of being locked into solid phases.

Almost all the fluid inclusions found in xenoliths probably are secondary (Roedder, 1965; Murck et al., 1978; Bergman, 1981), captured during crack healing and recrystallization of their host rocks (Evans and Wanamaker, 1983; Wanamaker and Evans, 1984). The fact that all of these inclusions are almost pure CO_2 rather than the CO_2-H_2O mixtures predicted by many researchers (see summary in Pasteris, 1987) attests that compositional changes have occurred in the original fluid (e.g., Mackwell and Kohlstedt, 1987). Two unusual exceptions are the presence of both H_2O and CO_2 in mantle inclusions from Ichinomegata, Japan (Trial et al., 1984), and Lake Nyos, Cameroon (Devine, 1987), as well as several mol% CO with CO_2 in inclusions from the Lunar Crater Volcanic Field, Nevada (Bergman and Dubessy, 1984). Regardless of whether the inclusions are primary or secondary, *if* (as is generally accepted) the volatile fugacities are buffered by the solid phases in the upper mantle and lower crust, then even late-stage fluids should reflect the inherent oxidation state of their host rocks. They clearly do not; under *P-T* conditions of the upper mantle and for an f_{O_2} along the fayalite-magnetite-quartz buffer, a C-O-H fluid would be dominantly CO_2, but also would have a considerable proportion of H_2O (Eggler and Baker, 1982).

The problem of explaining the pure CO_2 compositions of fluid inclusions in mantle xenoliths has been recognized previously (e.g., Mathez and Delaney, 1981; Bergman and Dubessy, 1984). Two possible explanations are the disproportionation of CO to CO_2 and graphite (found as a precipitate in xenoliths and basalts by Mathez and Delaney, 1981) or fractional distillation of gases evolved from the melt, which would purge the system first of CO and thus enrich the residuum in CO_2 (Mathez, 1984). Holloway and Jakobsson (1986) recently have discussed how the great contrast in solubilities of the different C-O-H volatiles in silicate melts can result in the eventual production of volcanic gases with f_{O_2} values about 1.5 log units more oxidizing than their mantle sources.

The present study concerns natural fluid inclusions in mantle rocks that re-equilibrated to new, externally imposed conditions in the laboratory. Monitoring of the changes in the fluid speciation and their dependence on temperature, f_{O_2}, and time places more stringent constraints on the mechanism of the changes in inclusion fluids during equilibration with external conditions. Such experiments also indicate how rapidly such re-equilibration can occur under geologically reasonable conditions. To our knowledge, this is the only study on the experimental re-equilibration of nonaqueous, volatile-bearing fluid inclusions. Pecher (1981) and Sterner and Bodnar (1985, 1986) have reported on the experimental re-equilibration of synthetic, brine-filled inclusions in quartz.

Experimental procedures

Description of samples

Fifteen separate single crystals of olivine (peridot) were investigated from type I mantle xenoliths from the San Carlos volcanic field in Arizona. Type I xenoliths probably represent portions of the wall of the mantle conduit (Irving, 1980) through which the alkali basalt at San Carlos erupted. The peridot has a compositional range of approximately Fo_{88} to Fo_{91}.

The peridot crystals were made into doubly polished chips approximately 1 mm thick and 1 cm by 1 cm in area. As shown in Figures 1A to 1I, several different kinds of internal features are present in the chips, and they differ among the chips. Several isolated fluid inclusions occur in each sample, usually widely dispersed but in many cases aligned along specific crystallographic directions or planes. The inclusions commonly are 8 μm or less in diameter (although some reach 20 μm) and are very difficult to see into because of their high relief and dark color (Fig. 1A). The optically clear central portions of the inclusions commonly are less than 6 μm. No glass inclusions are observed nearby. In some cases, however, the original fluid inclusions have decrepitated during the rise of the xenolith. This process has left a central cavity surrounded by a fracture plane coated with a thin film of fluid. Where partial healing of the fracture has occurred, an array of second-generation inclusions exists. Other inclusions decrepitated during the experiments described below (Figs. 1E, 1F). Minute (1–20 μm) euhedral flakes and rods of brownish spinel are dispersed in the same patterns and locations as the fluid inclusions in some samples (Figs. 1G, 1H, 1I). Several of the larger spinel grains also apparently contain fluid inclusions (Fig. 1B). In one chip (Fig. 1I), the finer spinels appear to be decorating the decrepitation planes surrounding burst fluid inclusions.

Description of experiments

The polished chips were heat-treated in a gas-mixing furnace at 1-bar pressure and several temperatures up to 1400 °C for 1 to 161 h (see Table 1). The samples were supported in the furnace either (1) by an alumina crucible lined with San Carlos olivine and suspended by a Pt wire (samples SC 103, 105, 201) or (2) by a shallow Pt cup or Pt wire attached to an alumina rod suspended from the top furnace fitting. At the end of each run, the chips were rapidly brought to room temperature by removing the sample assembly through the top of the furnace, resulting in unobstructed exposure to the air. The oxygen fugacity in the furnace was controlled for each experiment by mixing appropriate volumes of H_2 and CO_2 or CO and CO_2 at a total flow rate of 100 cm³/min (Deines et al., 1974). In order to remain within

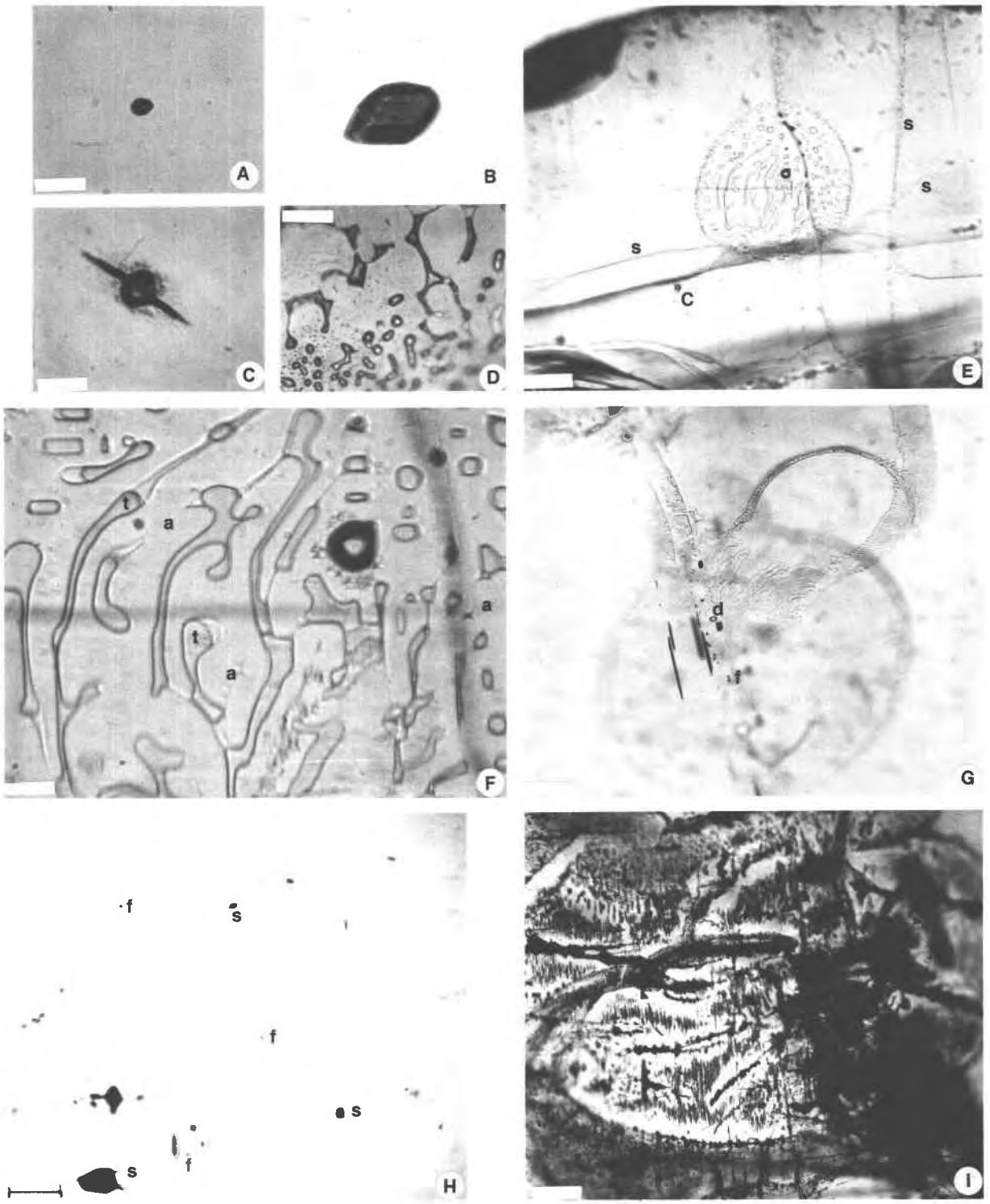

Fig. 1. (**A**) Isolated, intact fluid inclusion containing pure CO_2. Untreated sample SC307. Scale bar = 30 μm. (**B**) Yellow-brown (appears black), isolated spinel containing apparent fluid inclusions. In untreated sample SC307, a few hundred micrometers from Fig. 1A. Scale bar = 30 μm. (**C**) Inclusion 14 after first experiment on sample SC103B. Two elongated black fins are fractures, probably induced by stretching of inclusion during heating. Minute, secondary fluid inclusions ring original inclusions. Central, larger inclusion contains both CO_2 and CO. No Raman signal for graphite. Scale bar = 30 μm. (**D**) For comparison, an array of secondary fluid inclusions along curved fracture plane in natural, unannealed pyroxene grain in mantle xenolith from Kilbourne Hole, New Mexico. Scale bar = 30 μm. (**E**) Looking down onto plane of partially annealed decrepitation fea-

the f_{O_2} stability field for the natural olivine (Nitsan, 1974), the furnace atmosphere was maintained approximately between the iron-wüstite (IW) and wüstite-magnetite (WM) buffers. In spite of these precautions, samples that had undergone long heat treatment in the presence of Pt showed Fe diffusion and precipitation on the chip surface as either an oxide or metal phase (cf. Kohlstedt and Mackwell, 1987). We assume that any chemical effects of the Pt would have only a secondary effect on the fluid reequilibration.

In all but one case, the experiments involved treatment at an f_{O_2} lower than that reflected by the composition of the fluid in the inclusions in the olivine chip. The exception is run SC103B, which initially was equilibrated at an f_{O_2} between IW and WM, but subsequently was run at much higher f_{O_2} values; LRM analysis was done at the completion of each of the two experiments. For many of the olivine samples, a single chip was treated under the same conditions in several steps for differing lengths of time in order to permit MT monitoring of the reaction progress in the inclusions (see Wanamaker, 1986). The MT and LRM analyses reported in Table 1 were done only at the completion of the entire set of steps. However, since some of the chips were treated for much shorter lengths of time and at lower temperatures than others, the LRM analyses permit some evaluation of reaction rates and progress.

Analytical techniques

Both intact and decrepitated fluid inclusions in San Carlos olivine samples were analyzed by microthermometry (MT) and laser Raman microprobe (LRM) spectroscopy. A much larger suite of olivine samples and inclusions was analyzed by MT alone (Wanamaker, 1986). Standard microthermometric techniques were used, e.g., in determining equilibrium melting and homogenization temperatures and in calculating accuracy and reproducibility (Roedder, 1972; Hollister and Crawford, 1981). Microthermometry was done (by B.J.W.) on a Chaix-Meca heating-freezing stage, calibrated against the melting of apparently pure CO_2 inclusions in mineral standards. For peridot from one experimental run, the microthermometry was carried out in separate laboratories by Wanamaker and Pasteris, as an independent check on accuracy and reproducibility. Pasteris used a modified SGE-USGS stage (Pasteris, 1983) calibrated against pure organic liquids. Because of the varying degrees of difficulty in seeing into individual fluid inclusions, especially for the thick mineral plates used in this study, the accuracy and precision in recording the phase changes differ among the inclusions (see Wanamaker, 1986). In most cases, the accuracy and precision of the analyses are within ±0.4 °C. The melting temperatures for those inclusions studied by both authors in most cases agree within the stated error limits.

Inclusions in both treated and untreated San Carlos olivine samples were analyzed with a 1983 model RAMANOR U-1000 laser Raman microprobe (Instruments, SA), which permits the spectroscopic analysis of covalently bonded species in solid, liquid, and gas samples as small as about 2 μm (see, e.g., Rosasco and Etz, 1977; Dhamelincourt et al., 1979). The analytical conditions were excitation by the 514.5-nm line of an Ar^+ laser, approximately 10-mW laser power at the surface of the rock wafer, spectral steps of 0.5 cm^{-1}, and counting times of 10 s per point. The microscope objectives used are a 40× Nachet (N.A. = 0.75), an 80× Nachet (N.A. = 0.90), and a 160× Leitz (N.A. = 0.95).

The analytical reproducibility and limits of detection for LRM analyses are strongly dependent on the size of the fluid inclusion, its depth below the surface of the mineral grain, the optical properties of the inclusion and its host, as well as the concentration of the species of interest. For the inclusions analyzed in this study, the reproducibility of the individual LRM analyses is estimated to be about ±5 mol% CO, accuracy to be about ±7 mol% CO, and limits of detection to be about 2- to 3-bars partial pressure for each of the volatiles investigated (see Discussion). Derivation of the above factors as well as the method of deriving molar proportions of species from their Raman spectra are described in detail in Wopenka and Pasteris (1986, 1987) and Pasteris et al. (1988). The LRM spectra in Figure 2 show total counts plotted against frequency, in terms of wavenumber, i.e. cm^{-1}.

Results

Microthermometric results

Before heat treatment, the inclusions in the San Carlos olivine samples had melting temperatures of −56.6 ± 0.5 °C, indicative of pure CO_2. Their homogenization temperatures (T_h) indicate a range of initial densities from about 0.91 to 1.05 g/cm^3 and final densities (after heat treatment) as low as about 0.5 g/cm^3 (Vukalovich and Altunin, 1969). After heat treatment at controlled f_{O_2}, most of the original, intact fluid inclusions showed depressions in their melting points, compared to their original values (Table 1). Most inclusions also showed changes in their T_h values. In some of the experiments involving step-wise treatment, the T_h values initially decreased and then increased in succeeding steps (Wanamaker, 1986).

Optical examination of the samples after the experiments confirmed that the intact fluid inclusions have no fractures connecting them to the surface of the sample

←

ture in sample SC103B. Large, dark-rimmed central circle in cavity of original fluid inclusion (no. 31). Some secondary, dark fluid inclusions line fracture to right of center. Isolated fluid inclusion C is labeled. Other trails of minute fluid inclusions along subgrain boundaries and fracture are faintly visible (labeled s); gave no Raman signal for gases. Scale bar = 100 μm. (**F**) Enlargement of Fig. 1E, showing cavity of original fluid inclusion (dark-walled, circular). No Raman signal for graphite. Irregular tubules are the pores still remaining after partial annealing. Darker gray areas of tubules (t) are filled with liquid. Colorless areas are vapor filled; no Raman signal for volatiles from either phase. Intertubule colorless regions show where the fracture has been healed, i.e., annealed (a). Scale bar = 30 μm. (**G**) Untreated peridot sample SC401. Circular features are edges of unannealed decrepitation fractures. Parallel lineations are lined with several thin spinel rods (black), a cavity (d) from decrepitated fluid inclusion (larger, dark-rimmed ellipse), and several smaller, filled fluid inclusions (f). Scale bar = 100 μm. (**H**) Untreated peridot sample SC307. Most of opaque, larger bodies are brown spinels (s). Some of smallest black dots are fluid inclusions (f). Photographs 1A and B are enlargements of this field. Scale bar = 200 μm. (**I**) Untreated sample SC401, area near that in Fig. 1G. Black spinels here appear to be decorating a decrepitation surface. Some spinels at center of field have formed chains of square crystals linked by corners. Scale bar = 100 μm.

TABLE 1. Representative microthermometric and Raman microprobe data

Inclusion	T_m* (°C)	T_h** (°C)	LRM % CO	LRM Gr†	ν_1 CO_2	ν_2 CO_2	$\Delta\nu$ CO_2
Sample 103B (first experiment): 1400 °C, H_2-CO_2 mixture, log f_{O_2} = −8 ± 1, 161 h, 36% ± 20% CO (calc.)							
C	—	—	47	no	1285	1388	103
D	—	—	44	—	1284	1387	103
E	—	—	45	—	1284	1387	103
14	−61.5	v	41	—	1284	1387	103
15	−62.0	v	42	—	1284	1387	103
24	−61.2	—	28	—	1284	1387	103
31	−62.4	—	43	—	1284	1388	104
19	—	—	45	—	—	1387	—
Avg.‡	−61.9	v					
Sample 103B (second experiment): 1400 °C, H_2-CO_2 mixture, log f_{O_2} = −6 ± 0.5, 72 h, 7% ± 2% CO (calc.)							
A-1	—	—	ND	no	1285.5	1388.0	102.5
C	—	—	ND	—	1283.5	1386.5	103.0
31	—	—	ND	—	1282.5	1386.0	103.5
19	—	—	ND	—	—	1388	—
Avg.‡	−57.7	v					
Sample 101: 1200 °C, H_2-CO_2 mixture, log f_{O_2} = −11 ± 1, 1 h, 47% ± 22% CO (calc.)							
A-1	—	—	10	no	1281.0	1385.5	104.5
B-1	—	—	11	no	1281.5	1386.0	104.5
C-1	—	—	10	no	—	1385.5	—
Avg.‡	−59.1	l					
Sample 105: 1075 °C, H_2-CO_2 mixture, log f_{O_2} = −12.8 ± 1, 1.5 h, 50% ± 25% CO (calc.)							
1-A-2	—	—	ND	—	—	1385.5	—
6	−57.0	−11.5, l	ND	no	—	1386.0	—
Avg.‡	−57.0	l					
Sample 201: 1282 °C, H_2-CO_2 mixture, log f_{O_2} = −10 ± 0.5, 101 h, 66% ± 9% CO (calc.)							
A-1	—	—	19	no	1281.5	1386.0	104.5
B-1	—	—	ND	—	1285.0	1387.5	102.5
B-2	—	—	Tr	—	1283.5	1387.0	103.5
Avg.‡	−59.9	l					
Sample 307A: 1400 °C, H_2-CO_2 mixture, log f_{O_2} = −6 ± 0.5, 113 h, 7% ± 2% CO (calc.)							
1	−57.8	+25.5, l	Tr	no	1282.5	1386.5	104.0
2	−57.8	+25.5, l	ND	—	1283.0	1386.5	103.5
Avg.‡	−57.9	+25.5, l					
Sample 403A: 1400 °C, H_2-CO_2 mixture, log f_{O_2} = −6 ± 0.1, 101 h, 7% ± 2% CO (calc.)							
1-A-1	—	—	ND	—	1285.0	1388.0	103.0
1-A-2	—	—	ND	—	1284.5	1388.0	103.5
Avg.‡	−57.7	+23.2, l					
Sample 601B: 1400 °C, H_2-CO_2 mixture, log f_{O_2} = −10 ± 0.2, 111 h, 87% ± 4% CO (calc.)							
3	—	—	ND	yes	—	—	—
6	−63.6	—	ND	yes	—	—	—
Avg.‡	−63.3	v					
Sample 602C: 1400 °C, CO-CO_2 mixture, log f_{O_2} = −6 ± 0.3, 111 h, 7% ± 2% CO (calc.)							
A-1	—	—	ND	no	—	1386.5	—
B-1	—	—	ND	—	—	—	—
C-1	—	—	ND	—	—	—	—
Avg.‡	−57.8	+28.8, l					
Sample 602D: 1400 °C, CO-CO_2 mixture, log f_{O_2} = −10 ± 0.5, 109 h, 90% ± 3% CO (calc.)							
1-A-1	—	—	42	yes	1282.0	1386.0	104.0
10	−63.6	—	39	yes	1282.5	1386.0	103.5
14	—	—	46	yes	—	1386.0	—
Avg.‡	−63.6	v					
Sample 701B: 1400 °C, H_2-CO_2 mixture, log f_{O_2} = −10 ± 0.2, 111 h, 87% ± 4% CO (calc.)							
14	−63.4	v	46	—	—	1386.0	—
15	—	—	ND	yes	—	1386.0	—
Avg.‡	−63.3	v					
Sample 701E: 1000 °C, CO-CO_2 mixture, log f_{O_2} = −12 ± 0.4, 125 h, 19% ± 8% CO (calc.)							
5	−56.9	—	ND	—	—	1386.0	—
6	−57.1	−17.9, l	ND	—	—	1386.0	—
B-4	—	—	ND	—	—	—	—
A-1	—	—	ND	no	—	1385.5	—
Avg.‡	−57.2	l					
Sample 602: untreated							
A	—	—	ND	no	1280.5	1385.0	104.5
Sample 100: untreated							
A	—	—	ND	—	1280	1386	106
B	—	—	ND	—	1280	1385	105

TABLE 1—*Continued*

Inclusion	T_m* (°C)	T_h** (°C)	LRM % CO	LRM Gr†	ν_1 CO_2	ν_2 CO_2	$\Delta\nu$ CO_2
C	—	—	ND	—	1280	1385	105
D	—	—	ND	—	1280	1385	105
			Sample 307: untreated				
B-C	—	—	ND	—	1281	1386	105
A-B	—	—	ND	—	1281	1386	105
A-A	—	—	ND	—	1281	1386	105
			Sample 401: untreated				
C-A	—	—	ND	—	1281	1386	105
A	—	—	ND	—	1280	1385	105
B	—	—	ND	—	1279	1385	106
C	—	—	ND	—	1280	1385	105
D	—	—	ND	—	1280	1386	106

Note: ND = not detected; — = not analyzed for; Tr = trace. Temperatures and log f_{O_2} values given in each heading are those that are experimentally imposed in the furnace. Compositions given in mole percent.

* Melting temperature of CO_2 solid.

** Homogenization temperature, to liquid (l) or vapor (v) phase.

† Detection of graphite by LRM.

‡ Average of microthermic values of all inclusions in a run.

and thus to the furnace gas. The inclusions remain isolated, but there are short fractures emanating from some of them (Fig. 1C), commonly accompanied by minute ($\sim$1 μm), apparently one-phase fluid inclusions. Clearly, there has been some stretching and possible leakage.

To demonstrate the kinds of phase changes observed during MT analysis of the treated olivine samples, two examples (SC103B and SC201) are discussed. In its initial low-f_{O_2} experiment, sample SC103B underwent a three-step heat treatment for a total of 161 h. A significant depression of the melting temperature ($\Delta T_m \approx -1.7$ °C) in the intact fluid inclusions already had occurred in SC103B after only 2 h of annealing. After a total of 65 h, the melting-point depression had reached about -3.0 °C. By the end of 161 h of annealing, the ΔT_m had tripled compared to the 2-h run, perhaps in part due to the somewhat lower f_{O_2} in the last 96 h of the run. After all three heat-treatment steps, the fluid inclusions that were studied in SC103B froze between about -85 and -95 °C. They showed either major recrystallization or the melting of *one* of the solid phases between about -66 and -63 °C. The darkness of the inclusions and their small size made observations difficult.

In contrast, the inclusions in sample SC201 all froze between about -70 and -74 °C. They also showed more complex recrystallization-melting phenomena, in three stages: in the -80s and -70s °C (probably true recrystallization to coarser grain size), between -70 and -65 °C (phase boundaries move, brightness of phase changes, perhaps owing to melting of *one* of the solids), and a major phase change just below the ~ -60 °C melting temperature (perhaps true polythermal melting in a complex system with only three coexisting phases). This complex phase behavior in sample SC201 resembles that described by Bergman and Dubessy (1984) for natural CO-CO_2 fluids in a composite mantle xenolith. The difference in the MT phenomena between samples SC103B and SC201 is probably due to differences in both CO content and bulk density of the two fluids. More *P-V-T-X* information on the CO-CO_2 system might clarify these phase changes.

No evidence was found for the presence of H_2O in the inclusions studied in the San Carlos olivine samples. A separate water phase is not visible along the inclusion walls. However, the latter appear so dark and thick that >20 vol% H_2O could be hidden there. In further confirmation of the lack of water, no melting of clathrate was observed during MT analysis.

Raman results

Approximately 50 inclusions in 15 different polished samples of olivine crystals were analyzed with the LRM (representative analyses in Table 1). Four of the samples had not been heat-treated, so their inclusions represent the original fluid compositions and densities. About 12 inclusions were analyzed for CO_2, CO, H_2S, CH_4, H_2, N_2, and SO_2. The remaining inclusions were analyzed only for CO and CO_2. Because H_2O is an extremely weak Raman scatterer, it was not analyzed for. In all of the unannealed samples, only CO_2 was detected (Fig. 2A).

As an example of the kinds of results derived by LRM analysis, two samples (SC103B and SC602D) are discussed in detail. Raman results for all the samples are tabulated in Table 1. Sample SC103B was analyzed for the above gases after each of two sets of experiments: the first at relatively low and the second at higher f_{O_2}. The corresponding Raman results are discussed below. Where possible, the same inclusions were analyzed after each run. After the first, low-f_{O_2} experiment, (only) CO was detected in addition to CO_2 in each inclusion. For seven of the eight inclusions analyzed after the first experiment, the Raman-derived compositions range from 41 to 47 mol% CO. These inclusions are compositionally indistinguishable: 44 $\pm$ 5 mol% CO (Table 1). However, inclusion 24, which physically appears the same as the others but has a somewhat higher melting point, gave reproduc-

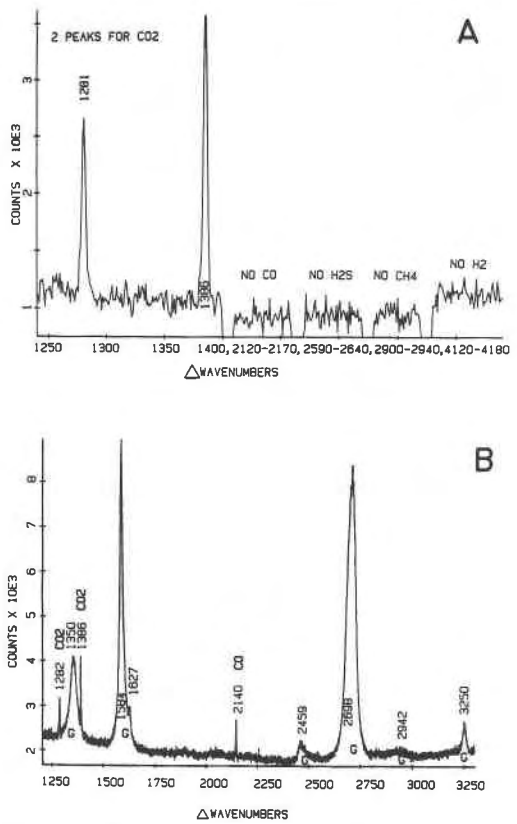

Fig. 2. Spectral conditions are discussed in text. (**A**) Raman analysis of 4-μm fluid inclusion C in area B of untreated olivine SC-307. Only CO_2 detected. Reference no. 370C1.DAT, J13. (**B**) Raman analysis of inclusion 10 in SC602D, annealed for 109 h at 1400 °C and log f_{O_2} of -10 ± 0.5. Relatively broad peaks for graphite (G) and much narrower peaks for volatiles CO and CO_2. Reference no. 602D-B1L, 602D-B1M.DAT, J61. See text for discussion.

ible compositions of about 28 mol% CO. The results of the first experiment therefore indicate that after 161 h at 1400 °C and log f_{O_2} of -8 to -9, the fluids in all but one of the isolated, intact inclusions that were analyzed in sample SC103B re-equilibrated to the same composition. Furthermore, re-equilibration began after only 2 h.

The correlation of about 44 mol% CO with about -5.5 °C T_m suggests a melting-point depression of about 1 °C per 8 mol% CO in the CO-CO_2 system. This is quite different from the correlation of 1 °C per 2–3 mol% CO derived by Bergman and Dubessy (1984), but their fluid inclusions had a density of about 1.0 g/cm^3, somewhat more dense than the present inclusions after heat treatment.

Because of the possible initial presence of graphite or its production in reactions during heat treatment of sample SC103B, this phase was carefully scanned for in an unannealed sample as well as in SC103B, particularly in dark-rimmed fluid inclusion 31. No graphite was detected, although the LRM can reveal graphite coatings on the order of several hundred angstroms in thickness (Pasteris and Wopenka, 1987). Various proportions of CO and a lack of graphite were also recorded by the LRM for several other samples run at different T-f_{O_2} conditions (Table 1).

The same sample SC103B was analyzed with the LRM after the second experiment at 1400 °C and log f_{O_2} of -6 ± 0.5. No CO was detected in the inclusions that previously had contained more than 40 mol% CO. In addition, the Raman signals for CO_2 were weaker than in the analyses done after the first experiment, and the specific positions of the Raman peaks for CO_2 had shifted for some inclusions. Both of these observations suggest some further decrease in internal pressure of the inclusion fluid between the first and second experiments (see Discussion).

Only one experiment was done on sample SC602D. LRM analyses on three inclusions in this sample gave Raman results of 39, 42, and 46 mol% CO. Within the limits of reproducibility of the LRM technique on inclusions of this size and optical clarity, these three inclusions are compositionally indistinguishable: 42 ± 5 mol% CO. Two other properties of the Raman spectra of this sample are significant: (1) Reference to the specific peak positions for CO_2 indicates that the internal pressures of the inclusions in this sample are unexpectedly high, given their high re-equilibration temperature (1400 °C; cf. 1200 or 1282 °C for other samples; see Discussion). (2) In spite of their high molar proportion of CO and their high internal pressure, the inclusions do not give the strong Raman signals obtained from inclusions of comparable size and depth in sample SC103B (after first experiment).

Both of the above observations can be explained (see Discussion) by the fact that graphite has precipitated on the walls of the inclusions in SC602D, as was revealed by LRM analysis (Fig. 2B). Only in samples SC602D, SC601B, and SC701B was graphite detected, although representative inclusions from all chips were checked with the LRM. Furthermore, it is not evident optically in the above three samples that graphite coats the inclusions. The small size of the inclusions in most samples and the large refractive index contrast between the fluid and the olivine give the inclusions in all samples relatively thick, dark rims. No carbonate phase was detected in the inclusions, in contrast to some natural graphite-bearing fluid inclusions in olivine from kimberlites and from troctolites of the Duluth Complex (Pasteris and Wanamaker, 1987).

Discussion

Interpretation of Raman analyses of fluids

The analysis and interpretation of these inclusions demonstrate several of the advantages of LRM analysis compared to other analytical techniques: excellent optical resolution, sensitivity to density and/or pressure differences, ability to analyze individual inclusions, and ability to estimate detection limits. The small size of some inclusions makes it very difficult to determine accurate melting and homogenization temperatures; the thickness

of the heating-freezing chamber limits the researcher to a 32× or 40×, long-working-distance objective. However, the LRM permits complete access to the sample, so that up to a 160× objective was used to analyze inclusions only a few micrometers in diameter. As indicated above, the LRM detected graphite in cases in which optical observations failed to distinguish it.

Because of the constraints of the phase rule, all pure CO_2 fluid inclusions with a coexisting liquid and vapor phase have an internal pressure of 64 bars at 25 °C. Inclusions that by this temperature already have homogenized to a one-phase liquid (in all untreated samples and samples treated at higher f_{O_2} values) or to a one-phase gas (true for some very stretched or leaky inclusions and for samples treated at very low f_{O_2} values) have pressures greater or less than 64 bars, respectively. The addition of CO to CO_2 also will change the above pressure values.

Bertran (1983) has shown that the exact spectral positions of and the spacing between the two Raman peaks for CO_2 (nominally at 1285.5 and 1388.0 cm^{-1} at 1 bar) are a function of pressure. As pressure increases, the position of the higher-frequency peak remains almost constant or shifts down slightly, whereas the lower-frequency peak shifts down more markedly. The separation between the peaks ($\Delta\nu$) thereby increases with pressure (Bertran, 1983).

For the inclusions in all four unannealed samples that were analyzed, the CO_2 peak positions have a separation of 104.5 to 106.0 cm^{-1}. Values of $\Delta\nu = 104.5$ cm^{-1} were found in samples SC101, annealed at 1200 °C, and SC201, annealed at 1282 °C (see Table 1). However, in sample SC103B (after first experiment), annealed at 1400 °C, seven of the eight inclusions analyzed had CO_2 peak positions at 1284 and 1387 cm^{-1}, i.e., $\Delta\nu = 103$ cm^{-1}. The re-equilibrated inclusions clearly have lower internal pressures than the original inclusions. As expected, there is a correlation between temperature of re-equilibration and internal pressure in an inclusion. This correlation is due to stretching of the inclusions by elevating their temperature while not concurrently increasing the confining pressure on the host mineral. An interesting exception to this correlation between re-equilibration temperature and internal pressure is sample SC602D, which was treated at 1400 °C, but which retains the CO_2 peak positions for a moderately high-density fluid ($\Delta\nu = 103.5$–104.0), as mentioned above. This effect probably is due to the precipitation of graphite, which decreases the volume in the inclusion and effectively elevates the internal pressure compared to what it would have been if the inclusion had only stretched (see Bergman and Dubessy, 1984).

The frequency shift for CO_2 is difficult to calibrate for exact pressures (Bertran, 1983); the important point is that all the CO_2 peaks were measured with the same spectrometer setting, making intersample comparisons possible. The recorded peak positions are accurate to about ± 1 cm^{-1} and reproducible to ± 0.5 cm^{-1}, which was the stepping interval used in this study. The amount of pressure change in a heat-treated sample does not seem to correlate with the CO-CO_2 ratio in individual inclusions, i.e., in sample SC103B (first experiment), inclusion 24 has the lowest CO/CO_2 ratio, but it is inclusion C that shows the lowest internal pressure.

The lack of detection of CO by LRM in many of the inclusions must be regarded with caution, especially in the cases in which these same inclusions exhibit a depression of their melting temperature. Because of the optical constraints on micro–Raman spectroscopy, the limits of detection for a species A are governed by the smallest number of molecules of A that can be detected in the focused irradiated volume in the sample. In other words, for an inclusion that is at least as large as the volume of the focused laser beam (several micrometers in diameter after penetrating the mineral host), the detectability of species A depends on both its concentration in the fluid and the density of the fluid. The combination of density and concentration in a volatile phase is actually partial pressure. In controlled experiments on glass capillaries and fluid inclusions with excellent optics (Wopenka and Pasteris, 1987), we determined our detection limits for CO_2 and CO to be about 1-bar partial pressure. As discussed above, the properties of the present samples are such that for those fluid inclusions with good optics, we estimate the detection limits to be 2- to 3-bars partial pressure for CO and for CO_2. Considering CO_2-dominant inclusions with densities of 0.8 to 1.0 g/cm^3, 3-bars partial pressure of CO at room temperature translates into 3 mol% to 1 mol%, respectively. Therefore, for the inclusions under study, a few mole percent CO in an inclusion should be detectable. However, the graphite coating on the inclusion walls caused relatively low count rates for inclusions in samples SC602D and SC601B. Poor inclusion optics and excessive depth of inclusions beneath the surface of the chip caused deterioration of the detection limits (i.e., elevated them above 2- to 3-bars partial pressure) in samples SC602C and SC701E, and to a lesser extent, in SC105 and SC201.

For inclusions with good optical properties, the limits of detection of an LRM could be exceeded in two different ways, i.e., too small of an inclusion volume and too low of a species concentration in an inclusion (see Wopenka and Pasteris, 1987; Pasteris et al., 1988). Some very thin films of fluid have been captured along the partially annealed decrepitation plane of SC103B shown in Figures 1E and 1F, which generate a minute vapor bubble upon cooling. No CO_2 or CO was detected by the LRM in these films even for counting times of 60 s per wavenumber. There also was no signal for CO_2, CO, H_2, or O_2 in the presumably low-density, round, 1-μm, secondary inclusions that formed along subgrain boundaries or dislocations centered on the decrepitated inclusions.

Interpretation of Raman analyses of graphite

As recorded in Table 1, graphite was detected by LRM in three samples: 601B, 602D, and 701B. There is a long history of the use of Raman spectroscopy to characterize graphitic and other carbonaceous materials (e.g., Tuinstra

and Koenig, 1970; Vidano and Fischbach, 1978; Nemanich and Solin, 1979; Lespade et al., 1982; Beny-Bassez and Rouzaud, 1985). Figure 2B is the Raman spectrum of inclusion 10 in sample SC602D, which illustrates the spectroscopic features of the precipitated graphite. Both the first-order (1200–1700 cm^{-1}) and second-order (2400–3300 cm^{-1}; overtone) Raman bands are useful in characterizing the degree of crystallinity of C, i.e., the crystallite size of graphite. Single crystals of graphite have the fewest as well as the sharpest bands of all the graphitic or carbonaceous materials. The ratios of the intensities of certain bands are a function of the crystallite size (Tuinstra and Koenig, 1970). The actual degree of crystallinity of the C, in turn, is a function of the nature of the precursor carbonaceous material (e.g., glassy C, aromatic hydrocarbon, C-O-H vapor) and the thermal history of the sample.

The spectrum in Figure 2B shows that graphite in the fluid inclusion from sample SC602D is moderately well crystallized, as would be expected for C precipitated from a fluid phase at 1400 °C. The well-crystallized nature of the graphite is revealed by the fact that the most intense first-order peak is at 1584 cm^{-1} and that this peak shows only a shoulder at 1627 cm^{-1}. In general, as the degree of crystallinity of graphite decreases, i.e., the crystallite size decreases, the 1584 cm^{-1} peak broadens and shifts toward higher wavenumbers. Although the present sample clearly is well crystallized, it is not single-crystal graphite, as shown by the development of a strong Raman peak at about 1360 cm^{-1}. This peak is associated with "disorder" in the graphite structure (Vidano and Fischbach, 1978).

In well-crystallized graphite, there are also three groups of second-order, overtone bands. These are all displayed in Figure 2B: a strong doublet at 2700 and 2735 (displayed as 2698 cm^{-1}) and weaker bands at 2450 and 3250 cm^{-1}. As the crystallite size decreases, these second-order features broaden and the fine structure on the 2710 band disappears (as in Fig. 2B); an additional feature develops at about 2950, as recorded at 2942 cm^{-1} in Figure 2B. The relative intensities and breadths of the second-order bands as well as the ratio of the intensities of the 1360 to the 1585 bands (0.26 in this case) indicate a crystallite size of about 200 Å (Tuinstra and Koenig, 1970; Nemanich and Solin, 1979; Lespade et al., 1982). It is interesting to note that the ratio of the intensities of the 2710 to the 1585 bands, as well as the fine structure on the 1585 band, looks like those for glassy carbons heat treated at 2600 °C (Vidano and Fischbach, 1978), i.e., much better crystallized than glassy carbons heated at 1400 °C (temperature of the present experiments).

Generation of CO-bearing inclusions

To our knowledge, Bergman and Dubessy's (1984) is the only previous report of the detection of CO in individual inclusions in mantle xenoliths, in their case, untreated natural samples. The inclusions in our study, however, clearly have undergone re-equilibration. In evaluating the results of the present experiments, two major questions must be addressed. (1) What is the mechanism by which a pure CO_2 fluid is converted to a mixture of CO and CO_2? (2) Are the compositions of the inclusions the same as those predicted for the temperature and f_{O_2} conditions of their respective experiments?

Determination of the mechanism of speciation change in the fluid involves consideration of (1) internal equilibration of the CO_2 fluid with the surrounding mineral, (2) response to the f_{O_2} gradient between the fluid inclusions and the furnace gas, and (3) response to the concentration gradient between the fluid inclusions and the actual gas species in the furnace. To fully define the one-phase (fluid) binary C-O system, three variables must be fixed; possibilities are P, T, f_{O_2}, and composition. Once three of these parameters are fixed (in our experiments, the first three), then the bulk composition of the fluid as well as its actual speciation are fixed and can be calculated. Therefore, in order to attain equilibrium with the lower f_{O_2} prevailing in the furnace gas, the bulk composition of a fluid inclusion must change.

The specifics of the proposed mechanism of re-equilibration are discussed in detail by Wanamaker (1986 and in prep.), and therefore are only summarized here. Although both gas-gas and gas-mineral reactions ultimately are responsible for the changes in speciation in the fluid inclusions, simple diffusion of volatiles (e.g., $H_2 + CO_2 = H_2O + CO$) to or from the inclusions probably was not the major mechanism of re-equilibration. The rapidity with which the re-equilibration process *begins* requires that the external f_{O_2} be communicated to the fluid inclusions by rapidly diffusing point defects and not by diffusion of gas species (Wanamaker et al., 1987). The fact that consistent fluid compositions were generated in the inclusions regardless of whether H_2-CO_2 or CO-CO_2 gas mixtures were used in the furnace further supports the argument against diffusion of specific gas species into the inclusions. In addition, the diffusivity of the point-defect species responsible for the re-equilibration is consistent with that measured for Mg and Fe vacancies in olivine (Nakamura and Schmalzreid, 1984). The exact composition of a re-equilibrated fluid inclusion and the rate at which that composition is finally attained probably depend on the solubility of point defects in the surrounding olivine (i.e., its buffering capacity) and on the slower lattice diffusion of atomic species away from the inclusion once the olivine's solubility limits have been exceeded.

The specific compositions of the inclusions are another matter of consideration. Figure 3 is a plot of MT final melting temperatures of the fluid inclusions vs. the relative oxygen fugacity imposed on them by the furnace atmosphere (expressed as number of $\log f_{O_2}$ units below that of the FMQ buffer). Each data point represents several inclusions in a single olivine sample. The points are labeled with two values of mol% CO (in a CO-CO_2 mixture): the value calculated for the T-f_{O_2} conditions in the furnace [in brackets] and the average value derived from LRM analyses of individual inclusions (in parentheses).

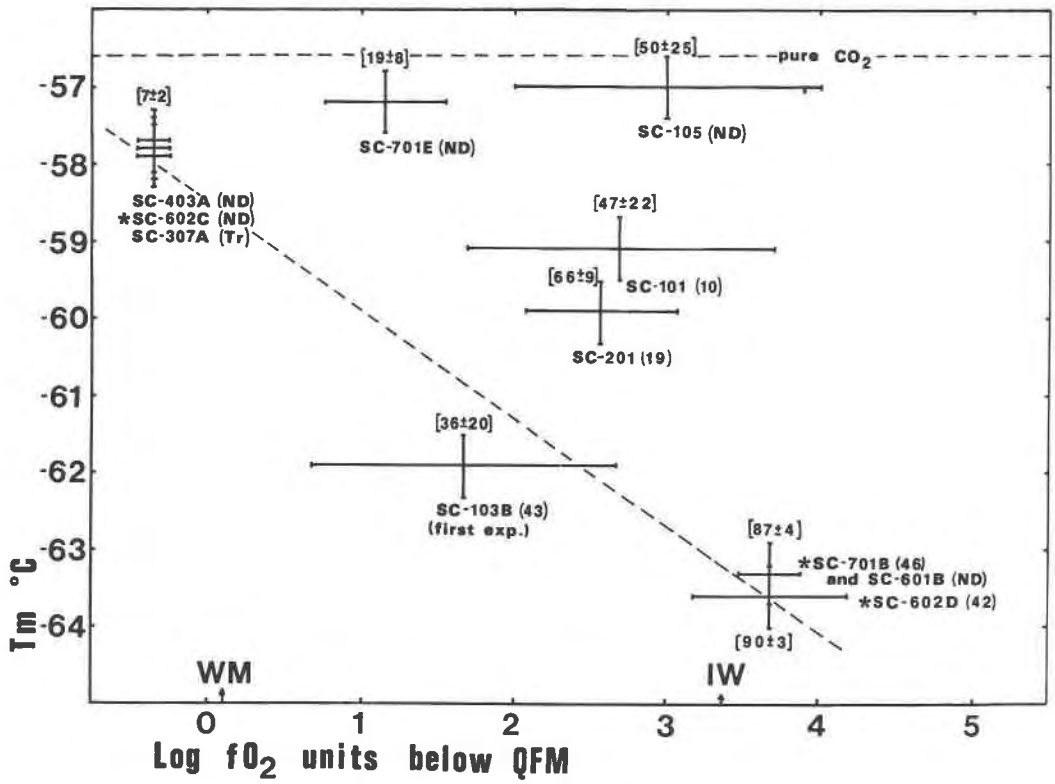

Fig. 3. Plot of melting temperature of fluid inclusions vs. furnace-imposed f_{O_2}, relative to FMQ ($\Delta \log f_{O_2}$). Vertical bars indicate range and uncertainty in MT values; horizontal bars for uncertainty in furnace f_{O_2}. Asterisks denote samples equilibrated with CO-CO_2 gas mixtures; all others treated in H_2-CO_2 mixtures. Values in brackets are mol% CO calculated for CO-CO_2 fluid at 5–10 kbar in equilibrium with imposed f_{O_2}. Values in parentheses are mol% CO derived from LRM analyses on inclusions. Arrows along x axis show f_{O_2} of wüstite-magnetite (WM) and iron-wüstite (IW) buffers at 1400 °C and 1 bar. Dashed line is linear regression to data points for seven samples treated at 1400 °C.

The calculated CO compositions are for 5- to 10-kbar pressure and the appropriate experimental temperatures for the equilibrium $2CO_2 = 2CO + O_2$, which is believed to be the dominant reaction within the inclusions. Details of the gas-mixing model and calculations are presented in Wanamaker (1986); the results at 1 bar from this model match those of Deines et al. (1974) at 1 bar. As stated above, the inclusions have a range of both initial and final densities. Five- to ten-kilobars pressure was chosen as a reasonable estimate for internal pressure in the unstretched inclusions at 1200 to 1400 °C. The calculations show that at a temperature of 1400 °C, the equilibrium CO content is about 20 mol% less at 1 bar than at 10 kbar for inclusions in the range of 10 to 75 mol% CO. At very high and very low concentrations of CO, there is less of a pressure effect.

From Figure 3, it is clear that there is a correlation between T_m and relative oxygen fugacity, and therefore between T_m and calculated CO content. However, except for the first experiment done on sample SC103B, there is a discrepancy between the calculated CO content and that derived from LRM analysis. We interpret these LRM-derived values as providing useful information on both the composition and state of equilibrium of the fluids in the samples. For example, the apparent low concentrations of CO that were derived from LRM analysis of SC101 and SC201 probably reflect the lack of complete equilibration of these samples. SC101 was treated for only 1 h, at the relatively low temperature of 1200 °C. Although SC201 was treated for 101 h, the temperature was only 1282 °C. The LRM analyses on inclusions in both of these samples are believed to represent the partial reaction of CO_2 to CO. The higher temperature (1400 °C) and longer run time (161 h) for SC103B probably account for the excellent correlation between the calculated (36 ± 20) and LRM-derived (44 ± 5) mole percents of CO in the fluid inclusions. We therefore conclude that the fluid inclusions (except for no. 24) in SC103B had completely equilibrated to the conditions imposed during the first experiment. However, Figure 3 also shows that no CO was detected by LRM in several sets of inclusions that have depressed melting temperatures. This discrepancy probably is due to the detection limits of the LRM, which were elevated by poor optics in some of the samples.

Samples SC601B (same run conditions as SC701B) and SC602D at first appear problematic, however. They were all run at 1400 °C for about 100 h, i.e., presumably sufficient for re-equilibration. Although the calculated CO

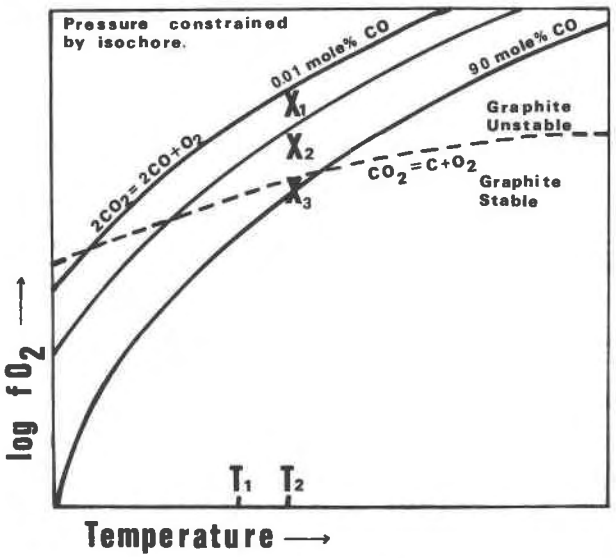

Fig. 4. Highly schematic diagram (after Bergman and Dubessy, 1984, Fig. 6b) of the T-f_{O_2} relationships of the reactions $2CO_2 = 2CO + O_2$ (occurring within inclusions) and $CO_2 = C + O_2$ (defining upper stability limit of graphite). Pressure not constant, but constrained by isochore (P-T trajectory) for specific fluid inclusion. For experiments done at constant temperature, such as T_2, as f_{O_2} is lowered from X_1 to X_2, mol% CO rises in the equilibrium C-O fluid. However, although f_{O_2} of furnace gas can be lowered to X_3 (90 mol% CO), f_{O_2} of fluid in inclusions becomes buffered by reactions $CO_2 = C + O_2$ and $2CO = CO_2 + C$ (mol% CO <90). At lower temperature, such as T_1, maximum CO content is buffered to even lower values than at T_2.

contents are 87 ± 4 and 90 ± 3 mol% CO, respectively, the LRM compositions are only about 40–46 mol% CO. This inconsistency is especially disturbing in that the very depressed T_m values, especially for SC602D, seem to confirm the presence of more CO than in sample SC103B (first experiment).

The key to this apparent inconsistency is the presence of graphite in samples SC601B, 701B, and 602D, but its absence in SC103B. As has been discussed by Muan (1958), French and Eugster (1965), French (1966), Eggler et al. (1979), Mathez (1984), Bergman and Dubessy (1984), and Kadik and Lukanin (1985), in the system C-O, the precipitation of graphite causes buffering of the f_{O_2}. The ramifications of graphite precipitation are shown by Figure 6b of Bergman and Dubessy (1984), specifically for their CO-CO_2 fluid inclusions, and are represented diagrammatically in Figure 4. The upper f_{O_2} limit of graphite stability is defined by the reaction $C + O_2 = CO_2$. This reaction has been plotted on the same T-f_{O_2} diagram as the reaction $2CO_2 = 2CO + O_2$, which is believed to be the controlling gas equilibrium in the fluid inclusions. A pressure must be specified for such a plot; in the case of a fluid inclusion, the pressure is constrained by some isochore (T-P trajectory), such as the isochore equivalent to a CO_2 density of 1 g/cm³. It can be seen that at elevated temperatures, such as 1400 °C, as the f_{O_2} of the C-O system is lowered, the CO content of the fluid increases. As f_{O_2} decreases considerably below FMQ, the field of graphite stability is reached. Once graphite precipitates (kinetic barriers overcome), then incremental decreases in external f_{O_2} no longer produce monotonic increases in the concentration of CO in the CO-CO_2 fluid. The fluid becomes self-buffered by the pair of reactions $2CO = CO_2 + C$ and $CO_2 = C + O_2$, i.e., along the CCO (graphite + fluid) buffer. In other words, the stability field of graphite precludes the attainment of CO-dominant fluids at moderate to high pressures (cf. Eggler et al., 1979; Mathez, 1984). The *theoretical* upper limit on CO concentration for any given experiment at 1400 °C is a function of the inclusion's internal pressure (density). The *actual* maximum content of CO is furthermore controlled by the kinetics of graphite precipitation.

It is significant that graphite did precipitate during these relatively short-term experiments, in that graphite is known to experience kinetic barriers to precipitation and decomposition (see discussion in Mathez and Delaney, 1981). According to the calculations of Eggler et al. (1979), at 1400 °C and 10 kbar, the maximum content of CO for a C-O fluid in equilibrium with graphite is 40 mol%. This value is in excellent agreement with the 42 ± 5 mol% CO content determined by LRM for the three graphite-bearing samples. Because the first experiment on SC103B (1400 °C, log $f_{O_2} = -8 \pm 1$) did not produce graphite, whereas samples SC601B, 602D, and 701B (1400 °C, log $f_{O_2} = -10 \pm 0.5$) all do have graphite, it appears that for the inclusion densities involved here, the upper limit of graphite stability at 1400 °C is about log $f_{O_2} = -9 \pm 1$ (cf. log $f_{O_2} \approx -6$ for FMQ at 1400 °C and 8 kbar). This compares to Bergman and Dubessy's (1984) calculation that at 1400 °C, graphite is stable below a value of log f_{O_2} of about −7.5 for an inclusion with an equivalent-CO_2 density of 1.03 g/cm³. Our inclusions are less dense than this owing to stretching. If graphite had precipitated in the inclusions treated at lower temperatures, the equilibrium CO concentrations would have been less (see Fig. 4): for 1250 °C, about 20 mol% CO at 10 kbar and about 25 mol% CO at 8 kbar (Mathez, 1984).

There is an additional significance to the agreement between the CO contents that were calculated thermodynamically by Eggler et al. (1979) and those derived from LRM analyses on actual inclusions. The CO concentrations in C-O inclusions at room temperature and low pressure, i.e., the conditions of the LRM analyses, apparently are the same as those that pertain at 1400 °C and 10 kbar, as predicted by Bergman and Dubessy (1984). In contrast, in experiments concerning the equilibration of CO-CO_2 fluids with silicate melts, Eggler et al. (1979) found that the CO_2 concentration in the coexisting fluid was much higher than what they had predicted for a pure C-O fluid alone. This effect presumably is due to re-equilibration at lower temperature and pressure as well as to the higher solubility of CO than CO_2 in silicate melts (Holloway and Jakobsson, 1986). The system studied by Eggler et al. (1979) is clearly more complex than the one in the present suite of inclusions.

Inferences for the CO-CO_2 phase diagram

Relatively few *P-V-T-X* data are available on the CO-CO_2 system (see, e.g., Kaminishi et al., 1968; Christiansen et al., 1974), certainly not enough information to construct a *P-T* diagram contoured with isochores. However, the available data on the two end-member systems and interpretation of the above MT and LRM findings permit some inferences to be drawn. Because both the triple point and critical point of CO lie at lower temperatures than those for CO_2, the configuration of the *P-T* diagram for CO-CO_2 topologically should resemble that for CH_4-CO_2 (see Burruss, 1981; Heyen et al., 1982). In the step-wise heat treatment of some of the San Carlos olivine samples in the present study, the inclusions showed an initial decrease in T_h and then a subsequent rise in T_h. This would be expected for a *P-T* topology like that of CH_4-CO_2: if inclusion density remains essentially constant, an increase in mol% CO will lower the T_h. As the inclusion subsequently stretches and the density of the fluid decreases, the T_h will rise.

In spite of being stretched by heat-treatment, the most CO_2-rich inclusions still homogenize to the liquid phase. The fact that high-CO inclusions—with internal pressures (confirmed by LRM) comparable to those in CO_2-rich inclusions—homogenize to the vapor phase suggests that isochores in the CO system are steeper than in the CO_2 system.

As noted above, the re-equilibrated fluid inclusions in samples SC601B and 602D had melting temperatures lower than those for SC103B, although all three samples have about 42 ± 5 mol% CO. As explained in detail by Burruss (1981), the melting temperature of a fluid inclusion in a binary system is a function of *both* density and composition. The higher internal pressures (and probably densities) in the inclusions in SC601B and 602D (shown in 602D by LRM) compared to those in SC103B, caused the former to have lower melting temperatures. Again, this is what would be expected for the CO_2-rich region of a binary system analogous to CO_2-CH_4.

Clearly, MT alone leads to an erroneous interpretation of the compositions of these inclusions, namely that a decrease in T_m correlates with (1) an increase in mol% CO and (2) a decrease in internal f_{O_2}. The ability of LRM to quantify both composition and density of a fluid provides the explanation for the misleading MT observations.

Significance to mantle xenoliths

This set of controlled experiments proves the feasibility of the graphite-precipitation mechanism ($2CO = C + CO_2$) proposed by Mathez and Delaney (1981) for graphite-bearing fluid inclusions in some mantle xenoliths. This mechanism also may be applicable to the "primary igneous graphite" reported in ultramafic xenoliths by Pineau et al. (1987) and Kornprobst et al. (1987). The LRM findings further emphasize Mathez and Delaney's (1981) point that density measurements on many xenolith inclusions will yield misleading pressure estimates. However, the applicability of this reaction to high-pressure (e.g., >40 kbar) mantle xenoliths remains limited. As recognized by Muan (1958), French and Eugster (1965), Mathez (1984), Bergman and Dubessy (1984), and Kadik and Lukanin (1985), the CO content of a C-O(-H) fluid in equilibrium with graphite is only significant at high temperature and low total pressure. Furthermore, although the inclusions studied here and those in most other xenolith studies appear to be limited to the C-O system, mantle fluids clearly are better described by the C-O-H system. As shown by Holloway (1981), in the presence of a C-O-H fluid, the graphite stability limit also depends on the C:O:H ratio and thus is sensitive to both f_{O_2} and f_{H_2}. In other words, the reactions occurring in *primary* fluid inclusions in xenoliths from deep in the upper mantle are probably more complex than those investigated here. It is possible that some mantle xenoliths whose f_{O_2} is below that of FMQ attain significant CO concentrations during events at moderate pressures. The CO may then disproportionate to graphite and CO_2 (Mathez and Delaney, 1981).

French and Eugster (1965) and Mathez and Delaney (1981) have also emphasized the importance of determining whether the C-O(-H) fluids are associated with crystalline graphite, as distinguished from amorphous organic matter or another carbonaceous material. The available thermodynamic data and the calculations above refer to crystalline graphite. The ability of LRM to characterize the degree of crystallinity of graphite (e.g., Tuinstra and Koenig, 1970; Beny-Bassez and Rouzaud, 1985) is very useful in this regard, as discussed above. Mathez and Delaney (1981) obtained less definitive data from the wavelength distribution of characteristic X-rays from the carbonaceous matter found in basalts and xenoliths, which they compared to similar spectra obtained on graphite standards. More recently, Mathez (1987) has inferred from energy-dispersive electron-microprobe analysis that some of the natural carbonaceous matter is graphite intercalation compounds.

Conclusions

The results of this study have both geologic and analytical significance. Analytically, it is clear that the LRM technique is superior to MT analysis in terms of being able to specifically identify the "contaminant" species in CO_2-rich inclusions. The LRM also is superior to MT in its ability to quantify the concentration of CO and the relative internal pressures of the inclusions, in the absence of *P-V-T-X* data on the CO-CO_2 system. However, the LRM also showed its limitations in that it detected no CO in several sets of inclusions that showed obvious depressions in their melting temperatures. Either the optics of these inclusions and/or the low partial pressures of CO prevented detection by the LRM. This is another example of why *both* LRM and MT analysis should be applied to fluid inclusions.

In contrast, Raman spectroscopy proved more sensitive than microscopic observation to the presence of

graphite in several sets of inclusions. In addition, the LRM provided a nondestructive means of pinpoint determination of the degree of crystallinity of the graphite.

Geologically, it is clear that the compositions of fluid inclusions can change through mechanisms other than by host-mineral fracturing with subsequent recapturing of new and old fluids. The experiments reported here demonstrate that even inclusions that remain physically intact may change their speciation to reflect externally imposed conditions. In some cases, this re-equilibration may be accompanied by the precipitation of new solids.

As predicted by other researchers in several previous papers, the precipitation of graphite can occur under conditions appropriate to the Earth's upper mantle. The coexistence of this graphite with a C-O fluid acts as an f_{O_2} buffer and prevents the formation of CO-dominant fluids even at very low-f_{O_2} external conditions (IW to WM).

In this study, the equilibrium CO concentrations produced in the originally pure CO_2 inclusions are those that are predicted thermodynamically. Furthermore, the CO concentrations depend on the f_{O_2} of the furnace atmosphere, regardless of whether that atmosphere is imposed by CO-CO_2 or H_2-CO_2 gas mixtures. The adjustment in f_{O_2} within the originally pure CO_2 inclusions is accomplished primarily by defect diffusion through the host olivine. In terms of gas equilibria, the controlling reaction is $2CO_2 = 2CO + O_2$.

The speciation changes documented in this study demonstrate that internal re-equilibration of fluid inclusions may occur very rapidly in nature and that the reactions are reversible. This means that the xenolith fluid inclusions that we now examine probably reflect the f_{O_2} of comparatively late-stage thermal events. There also might be somewhat different speciations between type I and type II xenoliths (cf. Bergman and Dubessy, 1984) because of their different thermal histories. This study is further confirmation that the almost total lack of CO and other species in inclusions now found in xenoliths does not preclude their earlier presence. It also documents very rapid precipitation of graphite from a fluid phase. The results of the present study suggest that at least in some cases, if we do *not* find graphite precipitated in C-O inclusions, then we can be reasonably certain that the host rock did not have its final equilibration in the graphite stability field.

Another ramification of the results of this study is the need for further caution in interpreting electrochemical measurements of minerals (Sato, 1972) in terms of intrinsic oxygen fugacity. It long has been recognized (see, e.g., Sato, 1972, 1984; Arculus, 1985) that defects and *minor* nonstoichiometries in minerals are what are being measured by this technique. This fact means that the measurements are sensitive even to minute amounts of contamination, e.g., the decrepitation of a few fluid inclusions in a sample (cf. Ulmer et al., 1987). Furthermore, the re-heating of a sample for intrinsic f_{O_2} analysis could equilibrate phases—and defects—that did not form and equilibrate together in the mantle (analogous to the pure-CO_2 inclusions within mantle olivines of a very low f_{O_2} signature).

Acknowledgments

The experimental work was carried out by Wanamaker while a graduate student at Princeton University and a Visiting Scholar at MIT. The help of Brian Evans, Tim Grove, and Lincoln Hollister is gratefully acknowledged. This work was supported financially in part by NSF grants EAR 8217341 and EAR 8218738 to Brian Evans and Lincoln Hollister, respectively, and by the Exxon Production Research Fund. The experimental aspects of this paper have benefited from many helpful discussions with David Kohlstedt and Steve Mackwell; discussions with John Holloway about gas equilibria also are appreciated. We thank Richard Arculus, Edmond Mathez, and Brigitte Wopenka for their comments on an earlier version of the paper, although we retain full responsibility for all observations and interpretations. Jeff Seitz is thanked for drafting some of the figures.

References cited

Andersen, T., O'Reilly, S.Y., and Griffin, W.L. (1984) The trapped fluid phase in upper mantle xenoliths from Victoria, Australia: Implications for mantle metasomatism. Contributions to Mineralogy and Petrology, 88, 72–85.

Arculus, R.J. (1985) Oxidation status of the mantle: Past and present. Annual Review of Earth and Planetary Sciences, 13, 75–95.

Arculus, R.J., Dawson, J.B., Mitchell, R.H., Gust, D.A., and Holmes, R.D. (1984) Oxidation states of the upper mantle recorded by megacryst ilmenite in kimberlite and type A and B spinel lherzolites. Contributions to Mineralogy and Petrology, 85, 85–94.

Beny-Bassez, C., and Rouzaud, J.-N. (1985) Characterization of carbonaceous materials by correlated electron and optical microscopy and Raman microspectroscopy. Scanning Electron Microscopy, 1985/I, 119–132.

Bergman, S.C. (1981) Fluid inclusions in xenoliths: Samples of the mantle metasomatic fluid? Geological Society of America Program with Abstracts, 13, 408.

Bergman, S.C., and Dubessy, J. (1984) CO_2-CO fluid inclusions in a composite peridotite xenolith: Implications for upper mantle oxygen fugacity. Contributions to Mineralogy and Petrology, 58, 1–13.

Bertran, J.F. (1983) Study of Fermi doublet ν_1-$2\nu_2$ in the Raman spectra of CO_2 in different phases. Spectrochimica Acta, 39A, 119–121.

Burruss, R.C. (1981) Analysis of phase equilibria in C-O-H-S fluid inclusions. In L.S. Hollister and M.L. Crawford, Eds., Short course in fluid inclusions, p. 39–74. Mineralogical Association of Canada, Toronto, Ontario.

Christiansen, L.J., Fredenslund, A., and Gardner, N. (1974) Gas-liquid equilibria of the CO_2-CO and CO_2-CH_4-CO systems. Advanced Cryogenic Engineering, 19, 309–319.

Deines, P., Nafziger, R.H., Ulmer, G.C., and Woermann, E. (1974) Temperature-oxygen fugacity tables for selected gas mixtures in the system C-H-O at one atmosphere total pressure. Earth and Mineral Sciences Experiment Station Bulletin 88.

Devine, J.D. (1987) Possible mantle metasomatism beneath the Cameroon volcanic line. EOS, 68, 455.

Dhamelincourt, P., Beny, J.-M., and Poty, B. (1979) Analyse d'inclusions fluides à la microsonde MOLE à effet Raman. Bulletin de Minéralogie, 102, 600–610.

Eggler, D.H. (1976) Does CO_2 cause partial melting in the low velocity zone of the mantle? Geology, 2, 69–72.

——— (1987) Solubility of major and trace elements in mantle metasomatic fluids: Experimental constraints. In M. Menzies and C. Hawkesworth, Eds., Mantle metasomatism, p. 21–41. Academic Press, London.

Eggler, D.H., and Baker, D.H. (1982) Reduced volatiles in the system C-O-H: Implications to mantle melting, fluid formation, and diamond genesis. In S. Akimoto and M.H. Manghnani, Eds., High-pressure research in geophysics, p. 237–250. Reidel, Dordrecht, Holland.

Eggler, D.H., Mysen, B.O., Hoering, T.C., and Holloway, J.R. (1979) The solubility of carbon monoxide in silicate melts at high pressures and its effect on silicate phase relations. Earth and Planetary Science Letters, 43, 321–330.

Evans, B., and Wanamaker, B.J. (1983) Mechanisms of crack healing in olivine. EOS, 64, 493.

French, B.M. (1966) Some geological implications of equilibrium between graphite and a C-H-O gas phase at high temperatures and pressures. Reviews of Geophysics, 4, 223–253.

French, B.M., and Eugster, H.P. (1965) Experimental control of oxygen fugacities by graphite-gas equilibriums. Journal of Geophysical Research, 70, 1529–1539.

Gerlach, T.M., and Nordlie, B.C. (1975) The C-O-H-S gaseous system, part I: Composition limits and trends in basaltic gases. American Journal of Science, 275, 353–370.

Green, D.H., Falloon, T.J., and Tayor, W.R. (1987) Mantle-derived magmas—Roles of variable source peroditite and variable C-H-O fluid compositions. In B.O. Mysen, Ed., Magmatic processes: Physicochemical principles, p. 139–154. Geochemical Society Special Publication no. 1.

Heyen, G., Ramboz, C., and Dubessy, J. (1982) Simulation des équilibres de phases dans le système CO_2-CH_4 en dessous de 50 °C et de 100 bars. Application aux inclusions fluides. Comptes Rendus, Académie des Sciences, Paris, 294, serie II, 203–206.

Hollister, L.S., and Crawford, M.L., Eds. (1981) Short course in fluid inclusions. Mineralogical Association of Canada, Toronto, Ontario.

Holloway, J.R. (1981) Compositions and volumes of supercritical fluids in the earth's crust. In L.S. Hollister and M.L. Crawford, Eds., Short course in fluid inclusions, p. 13–38. Mineralogical Association of Canada, Toronto, Ontario.

Holloway, J.R., and Jakobsson, J.R. (1986) Volatile solubilities in magmas: Transport of volatiles from mantles to planet surfaces. Journal of Geophysical Research, 91, D505–D508.

Irving, A.J. (1980) Petrology and geochemistry of composite ultramafic xenoliths in alkalic basalts and implications for magmatic processes within the mantle. American Journal of Science, 280-A, 389–426.

Kadik, A.A., and Lukanin, O.A. (1985) Mantle outgassing during melting: The role of carbon in fluid production in regions of basalt magma formation. Geochemistry International, 22, 25–35.

Kaminishi, G.-I., Arai, Y., Saito, S., and Maeda, S. (1968) Vapor-liquid equilibria for binary and ternary systems containing carbon dioxide. Journal of Chemical Engineering, Japan, 1, 109–116.

Kohlstedt, D.L., and Mackwell, S.J. (1987) High-temperature stability of San Carlos olivine. Contributions to Mineralogy and Petrology, 95, 226–230.

Kornprobst, J., Pineau, F., Degiovanni, R., and Dautria, J.M. (1987) Primary igneous graphite in ultramafic xenoliths: I. Petrology of the cumulate suite in alkali basalt near Tissemt (Eggéré, Algerian Sahara). Journal of Petrology, 28, 293–311.

Lespade, P., Al-Jishi, R., and Dresselhaus, M.S. (1982) Model for Raman scattering from incompletely graphitized carbons. Carbon, 20, 427–431.

Mackwell, S.J., and Kohlstedt, D.L. (1987) Diffusion of hydrogen in olivine: Implications for the presence of water in the mantle. EOS, 68, 417.

Mathez, E.A. (1984) Influence of degassing on oxidation states of basaltic magmas. Nature, 310, 371–375.

——— (1987) Carbonaceous matter in mantle xenoliths: Composition and relevance to the isotopes. Geochimica et Cosmochimica Acta, 51, 2339–2347.

Mathez, E.A., and Delaney, J.R. (1981) The nature and distribution of carbon in submarine basalts and peridotite nodules. Earth and Planetary Science Letters, 56, 217–232.

Muan, A. (1958) Phase equilibria at high temperatures in oxide systems involving changes in oxidation states. American Journal of Science, 256, 171–207.

Murck, B.W., Burruss, R.C., and Hollister, L.S. (1978) Phase equilibria in fluid inclusions in ultramafic xenoliths. American Mineralogist, 63, 40–46.

Mysen, B.O. (1983) Rare earth element partitioning between (H_2O + CO_2) vapor and upper mantle minerals: Experimental data bearing on the conditions of formation of alkali basalt and kimberlite. Neues Jahrbuch für Mineralogie Abhandlungen, 146, 41–65.

Nakamura, A., and Schmalzreid, H. (1984) On the Fe^{2+}-Mg^{2+} interdiffusion in olivine. Berichte der Bunsengesellschaft: Physical Chemistry, 88, 140–145.

Nemanich, R.J., and Solin, S.A. (1979) First- and second-order Raman scattering from finite-size crystals of graphite. Physical Review B, 20, 392–401.

Nitsan, U. (1974) Stability field of olivine with respect to oxidation and reduction. Journal of Geophysical Research, 79, 706–711.

Olafsson, M., and Eggler, D.H. (1983) Phase relations of amphibole, amphibole-carbonate, and phlogopite-carbonate peridotite: Petrologic constraints on the asthenosphere. Earth and Planetary Science Letters, 64, 305–315.

Pasteris, J.D. (1983) Adaptation of SGE-USGS heating-freezing stage for operation down to −196 °C. Economic Geology, 78, 164–169.

——— (1987) Fluid inclusions in mantle xenoliths. In P.H. Nixon, Ed., Mantle xenoliths, p. 691–707. Wiley, New York.

Pasteris, J.D., and Wanamaker, B.J. (1987) Use of the laser Raman microprobe to monitor reactions in individual fluid inclusions. Geological Society of America Abstracts with Programs, 19, 800.

Pasteris, J.D., and Wopenka, B. (1987) Use of a laser Raman microprobe to trace geological reactions. In R.H. Geiss, Ed., Microbeam analysis—1987, p. 205–209, San Francisco Press, San Francisco.

Pasteris, J.D., Wopenka, B., and Seitz, J.C. (1988) Practical aspects of quantitative laser Raman microprobe spectroscopy for the study of fluid inclusions. Geochimica et Cosmochimica Acta, 52, 979–988.

Pecher, A. (1981) Experimental decrepitation and re-equilibration of fluid inclusions in synthetic quartz. Tectonophysics, 78, 567–583.

Pineau, F., Javoy, M., and Kornprobst, J. (1987) Primary igneous graphite in ultramafic xenoliths: II. Isotopic composition of the carbonaceous phase present in xenoliths and host lava at Tissemt (Eggéré, Algerian Sahara). Journal of Petrology, 28, 313–322.

Roedder, E. (1965) Liquid CO_2 inclusions in olivine-bearing nodules and phenocrysts from basalts. American Mineralogist, 50, 1746–1782.

——— (1972) The composition of fluid inclusions. U.S. Geological Survey Professional Paper 440JJ.

Rosasco, G.J., and Etz, E.S. (1977) The Raman microprobe: A new analytical tool. Research/Development [now called Industrial Research and Development], 28, 20–35.

Ryabchikov, I.D., Schreyer, W., and Abraham, K. (1982) Compositions of aqueous fluids in equilibrium with pyroxenes and olivines at mantle pressures and temperatures. Contributions to Mineralogy and Petrology, 79, 80–84.

Sato, M. (1972) Intrinsic oxygen fugacities of iron-bearing oxide and silicate minerals under low total pressure. Geological Society of America Memoir 135, 289–307.

——— (1984) Intrinsic oxygen fugacities and point defects. EOS, 65, 277.

Schneider, M.C., and Eggler, D.H. (1986) Fluids in equilibrium with peridotite minerals: Implications for mantle metasomatism. Geochimica et Cosmochimica Acta, 50, 711–724.

Spera, F.J. (1981) Carbon dioxide in igneous processes: II. Fluid dynamics of mantle metasomatism. Contributions to Mineralogy and Petrology, 77, 56–65.

Spera, F.J., and Bergman, S.C. (1980) Carbon dioxide in igneous petrogenesis: I. Aspects of the dissolution of CO_2 in silicate liquids. Contributions to Mineralogy and Petrology, 74, 55–66.

Sterner, S.M., and Bodnar, R.J. (1985) Re-equilibration of fluid inclusions in quartz during laboratory-simulated burial and uplift of metamorphic terranes. Geological Society of America Abstracts with Programs, 17, 727.

——— (1986) Re-equilibration of fluid inclusions in quartz at elevated temperatures and pressures: The role of H_2O diffusion. EOS, 67, 407.

Taylor, W.R., and Green, D.H. (1987) The petrogenetic role of methane: Effect on liquidus phase relations and the solubility mechanism of reduced C-H volatiles. In B.O. Mysen, Ed., Magmatic processes: Physicochemical principles, p. 121–137. Geochemical Society Special Publication no. 1.

Trial, A.F., Rudnick, R.L., Ashwal, L.D., Henry, D.J., and Bergman, S.C. (1984) Fluid inclusions in mantle xenoliths from Ichinomegata, Japan: Evidence for subducted H_2O? EOS, 65, 306.

Tuinstra, P., and Koenig, J.L. (1970) Raman spectrum of graphite. Journal of Chemical Physics, 53, 1126–1130.

Ulmer, G.C., Grandstaff, D.E., Weiss, D., Moats, M.A., Buntin, T.J., Gold, D.P., Hatton, C.J., Kadik, A., Koseluk, R.A., and Rosenhauer, M. (1987) The mantle redox state: An unfinished story. In E.M. Morris and J.D. Pasteris, Eds., Alkalic rocks and kimberlites. Geological Society of America Special Paper 215, 5–23.

Vidano, R., and Fischbach, D.B. (1978) New lines in the Raman spectra

of carbons and graphite. Journal of the American Ceramic Society, 61, 13–17.

Vukalovich, M.P., and Altunin, V.V. (1969) Thermophysical properties of CO_2. Collets Publishers Limited, London.

Wanamaker, B.J. (1986) The kinetics of crack healing and the chemical and mechanical re-equilibration of fluid inclusions in San Carlos olivine. Ph.D. dissertation, Princeton University, Princeton, New Jersey.

Wanamaker, B.J., and Evans, B. (1984) Experimental diffusional crack healing in olivine. In R.N. Schock, Ed., Point defects in minerals, p. 194–210. American Geophysical Union Geophysical Monograph 31.

Wanamaker, B.J., Kohlstedt, D.L., and Evans, B. (1987) Reequilibration of fluid inclusions in San Carlos olivine by point-defect diffusion. EOS, 68, 417.

Wendlandt, R.F., and Harrison, W.J. (1979) Rare earth partitioning between immiscible carbonate and silicate liquids and CO_2 vapor: Results and implications for the formation of light rare earth-enriched rocks. Contributions to Mineralogy and Petrology, 69, 409–419.

Wopenka, B., and Pasteris, J.D. (1986) Limitations to quantitative analysis of fluid inclusions in geological samples by laser Raman microprobe spectroscopy. Applied Spectroscopy, 40, 144–151.

——— (1987) Raman intensities and detection limits of geochemically relevant gas mixtures for a laser Raman microprobe. Analytical Chemistry, 59, 2165–2170.

Wyllie, P.J. (1980) The origin of kimberlite. Journal of Geophysical Research, 85, 6902–6910.

Manuscript received October 1, 1987
Manuscript accepted May 16, 1988